Spatial profile of dendritic calcium transients evoked by action potentials in rat neocortical pyramidal neurones

Jackie Schiller, Fritjof Helmchen and Bert Sakmann

Max-Planck-Institut für Medizinische Forschung, Abteilung Zellphysiologie, Jahnstrasse 29, D-69120 Heidelberg, Germany

1. Simultaneous measurements of intracellular free calcium concentration ($[Ca^{2+}]_i$) and intrasomatic and intradendritic membrane potential (V_m) were performed using fura-2 fluorimetry and whole-cell recording in neocortical layer V pyramidal neurones in rat brain slices.

2. Back-propagating action potentials (APs) evoked $[Ca^{2+}]_i$ transients in the entire neurone including the soma, the axon initial segment, the apical dendrite up to the distal tuft branches, and the oblique and basal dendrites, indicating that following suprathreshold activation the entire dendritic tree is depolarized sufficiently to open voltage-dependent calcium channels (VDCCs).

3. The $[Ca^{2+}]_i$ transient peak evoked by APs showed large differences between various compartments of the neurone. Following a single AP, up to 6-fold differences were measured, ranging from 43 ± 14 nM in the soma to 267 ± 109 nM in the basal dendrites.

4. Along the main apical dendrite, the $[Ca^{2+}]_i$ transients evoked by single APs or trains of APs had the largest amplitude and the fastest decay in the proximal region; the $[Ca^{2+}]_i$ transient peak and decay time constant following a single AP were 128 ± 25 nM and 420 ± 150 ms, respectively, and following a train of five APs (at 10–12 Hz), 710 ± 214 nM and 390 ± 150 ms, respectively. The $[Ca^{2+}]_i$ transients gradually decreased in amplitude and broadened in more distal portions of the apical dendrite up to the main bifurcation.

5. In the apical tuft branches, the profile of the $[Ca^{2+}]_i$ transients was dependent on AP frequency. Following single APs, the $[Ca^{2+}]_i$ transients in tuft branches were larger compared with those proximal to the main bifurcation, whereas $[Ca^{2+}]_i$ transients evoked by a train of APs showed no significant increase.

6. In oblique and basal dendrites, the $[Ca^{2+}]_i$ transients evoked by single APs or trains of APs had the largest amplitudes measured in the entire neurone. Following single APs, the mean $[Ca^{2+}]_i$ transient peak was 226 ± 69 nM in oblique dendrites, and 267 ± 109 nM in basal dendrites. Following a train of five APs, in both oblique and basal dendrites the $[Ca^{2+}]_i$ transient peak exceeded 1·5 μM in most neurones examined.

7. Experiments using voltage commands simulating AP wave shapes applied to the soma in the presence of tetrodotoxin (TTX) indicate that active dendritic AP propagation is essential for the generation of $[Ca^{2+}]_i$ transients in apical and basal dendrites.

8. It is suggested that the large differences in the amplitudes of AP-evoked $[Ca^{2+}]_i$ transients measured in different compartments of pyramidal neurones could differentially control the efficacy of synaptic transmission in different dendritic compartments, as well as the integration of postsynaptic potentials.

Neocortical layer V pyramidal neurones possess an elaborate dendritic tree composed of a long apical dendrite ending in a tuft of fine branches, and basal and oblique dendrites (White, 1989; DeFelipe & Farinas, 1992). The dendritic tree is the major recipient of excitatory and inhibitory synaptic inputs and determines the spatial and temporal integration of postsynaptic potentials depending on the location of the synapses and on the passive and active properties of the dendritic membrane (Rall 1967; Jack, Noble & Tsien, 1983; Spruston, Jaffe & Johnston, 1994).

Intracellular calcium may act as second messenger regulating membrane excitability, as well as synaptic integration and plasticity. Calcium ions act via different pathways, for example, they modify properties of ion channels and receptors such as K^+ channels (Blatz & Magleby, 1987; Lancaster & Nicoll, 1987; Lancaster & Zucker, 1994), glutamate and γ-aminobutyric acid (GABA) receptors (Inoue, Oomura, Yakushijii & Akaike, 1986; Mayer, MacDermott, Westbrook, Smith & Barker, 1987; Llano, Leresche & Marty, 1991). In addition, Ca^{2+} is thought to mediate the induction of long-term potentiation and depression (for review, see Artola & Singer, 1993; Bliss & Collingridge, 1993).

Stuart & Sakmann (1994) have shown that following suprathreshold stimulation of layer V pyramidal neurones, action potentials (APs) back-propagate into the main apical dendrite. Here we characterize the spatial and temporal profile of AP-evoked $[Ca^{2+}]_i$ transients along the entire neurone, concentrating on two main issues. First, whether synapses located at various portions of the dendritic tree are exposed to different AP-evoked $[Ca^{2+}]_i$ changes and second, whether dendritic voltage-dependent Na^+ channels and active dendritic AP propagation are necessary to mediate dendritic $[Ca^{2+}]_i$ transients.

METHODS

Slice preparation and electrophysiological recording

Brains were rapidly removed from 13- to 17-day-old Wistar rats killed by decapitation, and parasagittal 250–300 μm thick neocortical brain slices were prepared using a vibrating slicer (FTB Vibracut, Weinheim, Germany). Slices were maintained at 24 °C in oxygenated extracellular solution containing (mM): 125 NaCl, 25 $NaHCO_3$, 25 glucose, 2·5 KCl, 1·25 NaH_2PO_4, 2 $CaCl_2$, 1 $MgCl_2$, at pH 7·4 (Biometra, Göttingen, Germany).

Layer V pyramidal neurones were visually identified using infrared differential interference contrast (IR-DIC) video microscopy. Slices were mounted on an upright epifluorescence microscope (Axioskop FS, Zeiss, Oberkochen, Germany), equipped with a ×63 water-immersion objective (0·9 numerical aperture, Achroplan, Zeiss). The microscope was placed on a sliding table, allowing changes of the field of view during the experiment (Stuart, Dodt & Sakmann, 1993). All measurements were done on thick tufted layer V pyramidal neurones (Larkman & Mason, 1990). Whole-cell recordings were made from apical dendrites and cell bodies of the neurones as described previously (Stuart *et al.* 1993; Stuart & Sakmann, 1994). Somatic recordings were made with an EPC-7 amplifier (List, Darmstadt, Germany) using pipettes with 1·8–4 MΩ resistance. Dendritic recordings were made with an Axoclamp-2A amplifier (Axon Instruments) using 10–12 MΩ pipettes. The distance of the dendritic recording site from the soma was measured directly from the video monitor using an image processor (Argus 10, Hamamatsu, Japan). In dendritic and somatic recordings the pipette solution contained (mM): 115 potassium gluconate, 20 KCl, 4 Mg-ATP, 10 phosphocreatine, 0·3 GTP, 10 Hepes; and 150 μM fura-2 (pH 7·2). Experiments were performed at 24 or 34 °C. For experiments at 34 °C, slices were perfused with 'prewarmed' extracellular solution. Stimulation pulses and data acquisition were controlled using a VMEbus computer system (Motorola Delta series 1147, Tampa, USA). All materials were purchased from Sigma apart from aminophosphonovaleric acid (APV) (Tocris, Bristol, UK), 2,3-dihydroxy-6-nitro-7-sulphamoyl-benzo(*f*)quinoxalin (NBQX) (BASF, Ludwigshafen, Germany) and fura-2 (Molecular Probes, Portland, OR, USA).

Fluorescence measurements

Neurones were loaded with the Ca^{2+}-sensitive indicator dye fura-2 via the patch pipette. Following whole-cell 'break in', fluorescence measurements were started after 15–20 min in sites up to 200 μm from the filling pipette and after 40–60 min in sites far from the electrode. Fluorescence measurements were done with two slightly different systems. For excitation we used either a Xenon lamp (XBO75, Zeiss) in combination with interference filters (360/380 nm, bandwidth 10 nm; Omega, Brattleboro, VT, USA) positioned in a filter wheel (Lambda-10, Sutter Instrument Co., Novato, CA, USA) or a polychromatic illumination system selecting wavelengths via a diffraction grating (bandwidth 12 nm, T.I.L.L. Photonics, Munich, Germany). In the latter case, measurements were done using excitation wavelengths of 380 and 353 nm (isosbestic for fura-2 in our preparation). Excitation light was coupled to the microscope via a light guide. The beam splitter–emission filter combinations were FT425-BP500-530 (Zeiss) and DC400-LP410 (T.I.L.L. Photonics), respectively.

Fluorescence was measured with one of two thermoelectrically cooled slow-scan CCD cameras: a relatively slow camera (CH250A, 512 × 512 Chip TH7895B, pixel size 19 × 19 μm^2, readout rate 200 kHz; Photometrics, Tucson, AZ, USA), or a faster camera (ATC-5, 384 × 288 Frame Transfer Chip TH7893FT, pixel size 22 × 22 μm^2, readout rate 2 MHz; Photometrics). The CCD cameras were operated in two modes depending on the requirement of the experiment. In the 'spot' mode we defined small rectangular regions of interest (ROI) which included a well-focused area of the dendritic tree or soma. Dendritic ROIs were typically 10 μm in length and 2–5 μm in width; somatic ROIs were about 5 × 5 μm^2. The pixels included in ROIs were binned on-chip in both directions (CH250A) or on-chip in one direction and off-line in the other direction (ATC-5) to create one 'superpixel'. These superpixels have a higher signal-to-noise ratio than the same ROI averaged off-line (Lasser-Ross, Miyakawa, Lev-Ram, Young & Ross, 1991), but the spatial resolution within the ROI is lost. Background fluorescence was measured in corresponding ROIs of the same size. Attention was paid in choosing the appropriate background ROIs, as in the very fine branches of the dendritic tree the background fluorescence could reach up to 60% of the total fluorescence in the ROI. The background ROIs were located as close as possible to the cellular ROI lacking dye-containing structures. We focused up and down to ensure no out-of-focus structures were below or above the background ROI and in addition we checked that background signals were constant during stimulation. A correction for bleaching (less than 0·6% per second) was made for each ROI by performing control measurements without stimulation. Fluorescence acquisition rates in the spot mode were 10 Hz using the CH250A camera and up to 100 Hz using the ATC-5 camera.

In the 'street-scan' mode we used the ATC-5 camera. Long rectangular regions, typically up to 100 μm in length and 5 μm in width, were selected. These regions were binned on-chip in one direction only, thus keeping the spatial resolution along the soma–dendritic axis. With the ATC-5 camera, high time resolution fluorescence measurements were possible (up to 100 Hz acquisition rate). Selection of background ROIs and correction for bleaching

were done as in the spot mode. In both modes 2–4 sweeps were averaged. Fluorescence data acquisition was controlled by a second VMEbus computer system (VDIPS-500, TVIPS, Munich, Germany). Fluorometric and electrophysiological data acquisition was synchronized via TTL pulses.

High spatial resolution fluorescence images of the neurones were taken at 380 nm excitation with exposure times of 0·2–1·5 s. When needed, successive frames were taken at the end of the experiment and collaged off-line.

Conversion of fluorescence intensities to $[Ca^{2+}]_i$

Changes in fluorescence signals following neuronal activation represent the spatially and temporally averaged time course of the Ca^{2+}-bound fraction of fura-2. Conversion of fluorescence signals to $[Ca^{2+}]_i$ assumed equilibrium of fura-2 with intracellular Ca^{2+} and was done using one of two methods. In the single wavelength method measurements were done at 380 nm excitation and background-corrected signals were expressed as relative fluorescence change $\Delta F/F = (F_0 - F_{380})/F_0$, where F_0 is the baseline fluorescence and ΔF the change in fluorescence from baseline. $\Delta F/F$ was converted to $[Ca^{2+}]_i$ according to (Grynkiewicz, Poenie & Tsien, 1985; Jaffe, Johnston, Lasser-Ross, Lisman, Miyakawa & Ross, 1992; Lev-Ram, Miyakawa, Lasser-Ross & Ross, 1992):

$$[Ca^{2+}]_i = \frac{[Ca^{2+}]_{rest} + K_d \dfrac{\Delta F/F}{(\Delta F/F)_{max}}}{1 - \dfrac{\Delta F/F}{(\Delta F/F)_{max}}}, \quad (1)$$

where K_d is the dissociation constant of fura-2, $(\Delta F/F)_{max}$ is the saturation value of $\Delta F/F$ when fura-2 is completely bound to Ca^{2+}, and $[Ca^{2+}]_{rest}$ is the resting Ca^{2+} concentration determined using the ratio method with 360 and 380 nm excitation. Using the isosbestic ratio method, fura-2 was excited at 380 nm and the isosbestic wavelength, 353 nm. Isosbestic fluorescence measurements were made before and after stimulation. After background subtraction, the ratio $R = F_{353}/F_{380}$ was converted to $[Ca^{2+}]_i$ using the standard ratioing equation (Grynkiewicz *et al.* 1985):

$$[Ca^{2+}]_i = K_{eff}(R - R_{min})/(R_{max} - R), \quad (2)$$

where R_{min} is the ratio when fura-2 is completely unbound to Ca^{2+}, R_{max} when it is completely bound to Ca^{2+}. K_{eff} is the effective dissociation constant of fura-2 (see below).

All fluorescence measurements are presented as changes of $[Ca^{2+}]_i$ from the resting intracellular calcium concentrations ($\Delta[Ca^{2+}]_i$). Mean values are given as means ± S.D., and statistical significance was examined using Student's t test.

Determination of calibration constants

R_{min} and R_{max} were determined in cells according to Neher & Augustine (1992). Briefly, the patch pipette was used to equilibrate the cell with very high or low Ca^{2+} concentrations. The intracellular solutions contained either 20 mM EGTA or 50 mM $CaCl_2$ (pH was adjusted to 7·2) to obtain values for R_{min} and R_{max}, respectively (values were pooled from five cells). Care was taken during these experiments to keep low and stable access resistance recordings (less than 8 MΩ). R_{min} was between 0·41 and 0·6, R_{max} between 4·1 and 5·1. The K_d of fura-2 was estimated *in vitro* for the intracellular pipette solution using the Ca^{2+} calibration concentrate kit (Molecular Probes) and was 250 nM at 24 °C. According to Lattanzio & Bartschat (1991) the K_d of fura-2 decreases about 10% per 15 °C increase in temperature; therefore we used a K_d of 233 nM for measurements at 34 °C. Attempts were made to determine the K_d in cells by using an intermediate known Ca^{2+} concentration, but they were not sucessful, probably because of the difficulty of clamping the Ca^{2+} concentration in such large cells. Using the isosbestic method, K_{eff} was calculated as $K_{eff} = K_d(R_{max}/R_{min})$ (Neher & Augustine, 1992); otherwise it was obtained *in vitro* with calibration solutions. Resting $[Ca^{2+}]_i$ levels were found to be 53 ± 30 nM at 24 °C ($n = 19$). $(\Delta F/F)_{max}$ can be calculated as:

$$(\Delta F/F)_{max} = (K_{eff} - K_d)/(K_{eff} + [Ca^{2+}]_{rest}), \quad (3)$$

giving a value of about 87% for our conditions. This value is in good agreement with estimates from dye-saturating experiments in neurones.

RESULTS

Measurement of $[Ca^{2+}]_i$ transients evoked by back-propagating APs

Neocortical layer V pyramidal neurones were identified visually (Stuart *et al.* 1993) and simultaneous measurements of electrical activity and fluorescence were performed using whole-cell recording with patch pipettes and the Ca^{2+}-sensitive indicator dye fura-2 (Grynkiewicz *et al.* 1985). Neurones were loaded with 150 μM fura-2 via patch pipettes located at the soma or at various locations along the main apical dendrite. Figure 1*A* and *B* shows a representative example of $[Ca^{2+}]_i$ transients in the soma and the proximal apical dendrite following a single AP evoked by a brief current pulse injected via the somatic patch pipette. Fluorescence measurements were made in selected regions of interest, which were relatively small, well focused and read out as binned 'superpixels' ('spot' mode). Fluorescence measurements were converted to $[Ca^{2+}]_i$ off-line and are presented as changes over resting intracellular calcium concentration ($\Delta[Ca^{2+}]_i$). In both the somatic and the dendritic ROI, a single AP evoked a clear transient increase in $[Ca^{2+}]_i$ with a fast rise and a decay which could be well fitted with a single exponential. The $[Ca^{2+}]_i$ transient measured in the proximal apical dendrite was larger than that in the soma. In five neurones loaded via a somatic patch pipette the mean values of the $[Ca^{2+}]_i$ transient peak and decay time constant were 111 ± 51 nM and 630 ± 120 ms for dendritic ROIs (up to 120 μm from the soma), and 35 ± 5 nM and 1000 ± 400 ms for the somatic ROIs, respectively (using Student's paired t test: $P < 0·05$ for peak and decay time constant).

The differences in $[Ca^{2+}]_i$ transients between soma and proximal apical dendrite may indicate that soma and dendrites form different compartments with respect to the AP-evoked $[Ca^{2+}]_i$ transients. However, this observation may be influenced by a dye concentration gradient along the region measured and differential wash-out of endogenous Ca^{2+} buffers via the recording pipette. Two types of experiments were performed to examine these possibilities. First, neurones were loaded with fura-2 via

dendritic patch pipettes, to reverse a possible dye concentration gradient and endogenous buffer wash-out. Figure 1*C* and *D* illustrates that with dendritic filling also the $[Ca^{2+}]_i$ transient peak in the dendrite is larger and the decay time constant is smaller compared with the somatic one. The mean values of peaks and decay time constants in this loading configuration were 164 ± 43 nM and 380 ± 120 ms, respectively, for the dendrite and 48 ± 14 nM and 511 ± 170 ms, respectively, for the soma ($P < 0{\cdot}01$ for decay time constant and $P < 0{\cdot}001$ for peak, $n = 8$). In a second type of experiment, fura-2 was loaded simultaneously via two pipettes, one located at the soma, the

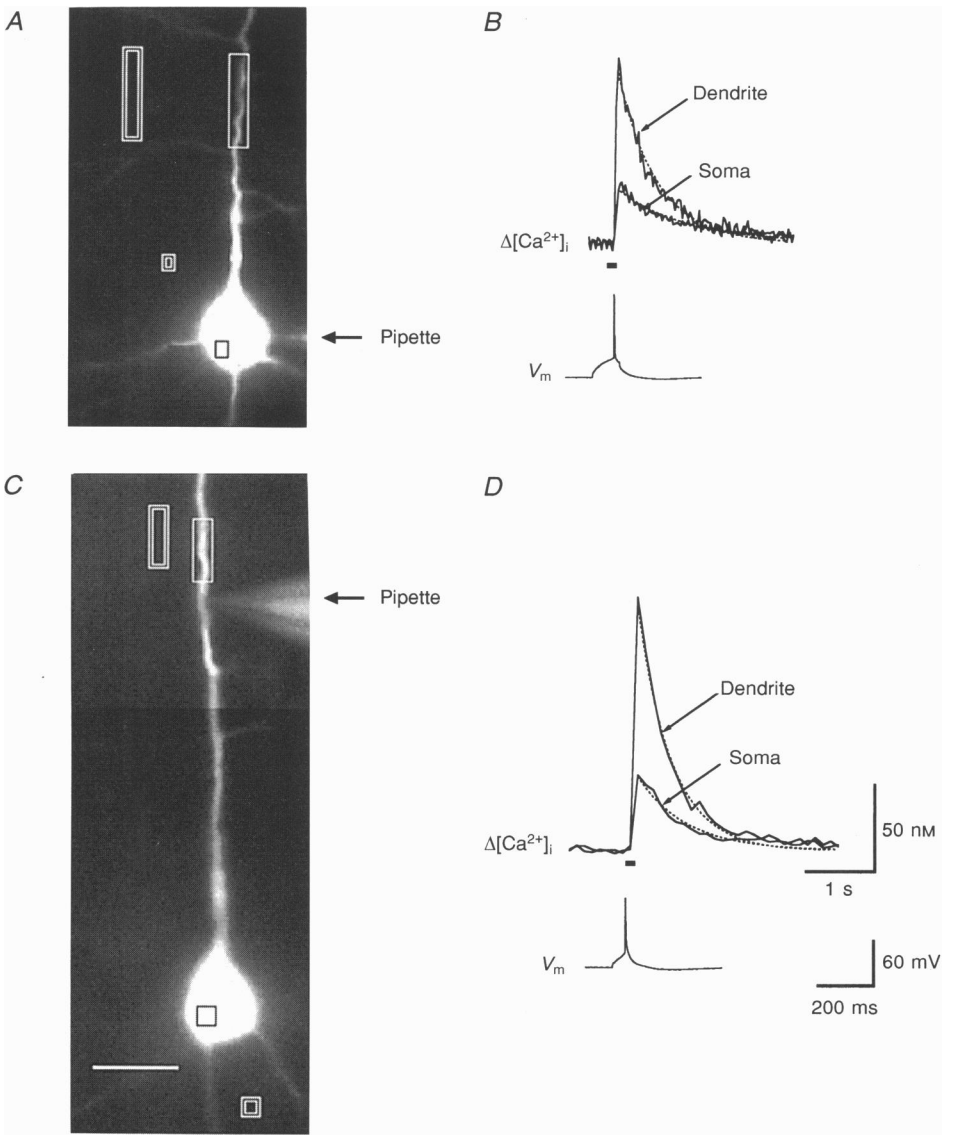

Figure 1. $[Ca^{2+}]_i$ transients in soma and dendrite of pyramidal neurones in rat neocortex evoked by single back-propagating APs

A, high spatial resolution fluorescence image (380 nm excitation) of a pyramidal neurone filled with fura-2 (150 μM) via a somatic patch pipette (arrow). Rectangles indicate somatic and dendritic ROIs (single border) and the corresponding background ROIs (double border). *B*, $[Ca^{2+}]_i$ transients in the dendritic and the somatic ROI evoked by a single AP (upper traces). The AP was evoked by a 100 ms current injection pulse to the patch pipette (lower trace, expanded time scale). $[Ca^{2+}]_i$ increase is significantly larger in the dendritic ROI compared with the somatic one. Fluorescence signals were acquired at 28 Hz in spot mode with the ATC-5 CCD camera. *C*, fluorescence image of a pyramidal neurone filled with fura-2 via a dendritic pipette located 120 μm from the soma (arrow). ROIs are indicated as in *A*. Scale bar (which also applies to *A*), 25 μm. *D*, $[Ca^{2+}]_i$ transients in the dendritic and the somatic ROI (upper traces) evoked by a single AP (lower trace, 50 ms current pulse). Fluorescence signals were acquired at 10 Hz in spot mode with the CH250 CCD camera. The scale bars in *D* also apply to *B*. Single exponential curves fitted to the data are shown as dotted lines. Here and in subsequent figures, the small filled bar marks the timing of the AP.

other at the apical dendrite (Fig. 2*A*). Figure 2*B* illustrates that the $[Ca^{2+}]_i$ transient in this loading configuration also differs significantly between soma and dendrite, being larger and faster in the dendrite. Similar results were obtained in three other neurones. The size and shape of $[Ca^{2+}]_i$ transients differs between the somatic and dendritic loading configurations. Both the somatic and dendritic $[Ca^{2+}]_i$ transients were smaller in amplitude and slower when the neuron was loaded via a somatic pipette, possibly resulting from the larger size of the somatic pipette. Nevertheless, our results clearly indicate that the differences between somatic and dendritic $[Ca^{2+}]_i$ transients were not caused by a dye concentration gradient or differential wash-out effects.

The AP-evoked $[Ca^{2+}]_i$ transients in both the soma and apical dendrite were blocked by 200 μM extracellular Cd^{2+} ($n = 3$), and were not affected by the addition of 200 nM NBQX and 100 μM APV ($n = 3$). These results suggest that $[Ca^{2+}]_i$ transients reflect predominantly Ca^{2+} entry via voltage-dependent calcium channels (VDCCs) present in the somatic and dendritic membrane, although a contribution of calcium release from internal stores.

To examine dendritic $[Ca^{2+}]_i$ transients under more physiological conditions, additional experiments were performed at 34 °C. For both somatic and dendritic ROIs the decay time constants of the $[Ca^{2+}]_i$ transients were reduced by about 45% at the higher temperature. Figure 2*C* summarizes the differences between the AP-evoked $[Ca^{2+}]_i$ transients in the somatic region (not including the nuclear region, see below) and the proximal dendrite (up to 120 μm from the soma) measured in the three loading configurations at room temperature (24 °C) and at 34 °C.

Summation of $[Ca^{2+}]_i$ transients during trains of APs

In vivo cortical neurones usually respond to a sensory stimulus by a train of APs (Alloway, Johnson & Wallace, 1993). To characterize dendritic $[Ca^{2+}]_i$ transients evoked by a train of APs, 400–500 ms depolarizing current pulses

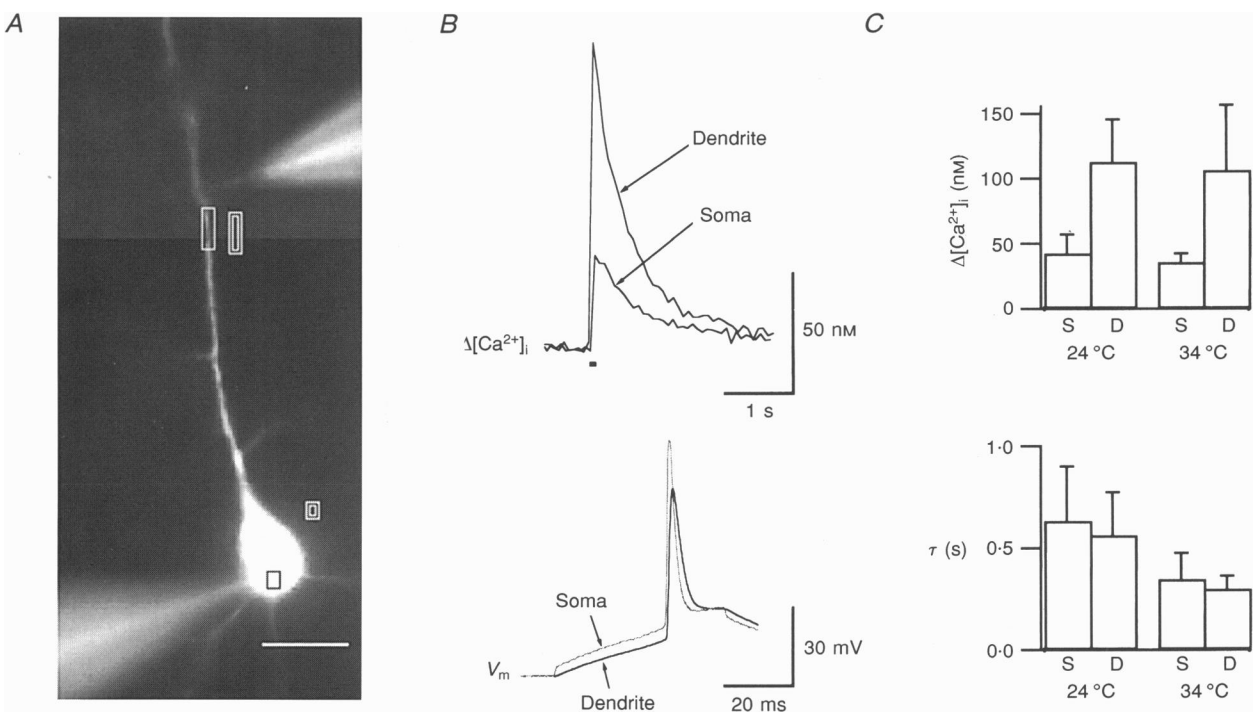

Figure 2. Simultaneous measurement of $[Ca^{2+}]_i$ and V_m from both main apical dendrite and soma

A neurone was loaded with fura-2 simultaneously via two patch pipettes located at the soma and the main apical dendrite (120 μm from the soma). Two ROIs were selected close to the recording pipettes. Fluorescence acquisition rate was 10 Hz. *A*, fluorescence image of the neurone showing the two ROIs (single border), background ROIs (double border) and the two pipettes. Scale bar, 25 μm. *B*, $[Ca^{2+}]_i$ transients evoked by a single AP measured in the dendritic and the somatic ROI (upper panel). APs were evoked by somatic or dendritic 50 ms current pulses for dendritic and somatic measurements, respectively. Lower panel illustrates simultaneous recording of somatic and dendritic APs, showing that the somatic AP precedes the dendritic one. Voltage traces are shown in expanded time scale. *C*, summary plot from 29 cells of the means of $[Ca^{2+}]_i$ transient peaks and decay time constants (τ) for non-nuclear somatic (S) and proximal apical dendritic (D) regions (20–120 μm from the soma) at 24 and 34 °C. Fluorescence acquisition rate for high temperature measurements was 100 Hz. Data are pooled from somatic, dendritic and double pipette experiments.

were injected via the recording pipette, resulting in a train of four or five APs showing frequency accommodation.

Figure 3*A* shows $[Ca^{2+}]_i$ transients evoked by a single AP or a train of five APs in the proximal apical dendrite. The train of APs elicited a larger increase in $[Ca^{2+}]_i$ due to summation of $[Ca^{2+}]_i$ transients, the single apparent peak being due to the limited time resolution of the fluorescence measurement (10 Hz acquisition rate). An example of $[Ca^{2+}]_i$ transients evoked by five APs measured at 10 and 100 Hz acquisition rates in the same dendritic ROI of the same cell is shown in Fig. 3*B*, and indicates that the peak of the $[Ca^{2+}]_i$ transient acquired at 10 Hz was underestimated by about 8% and that the decay time course is reliably measured.

Figure 3*C* illustrates the summation of $[Ca^{2+}]_i$ transients in the proximal apical dendrite during 4 s trains of APs with different rates (2, 10 and 20 Hz at 34 °C). APs were evoked by 5 ms current pulses injected via the recording pipette

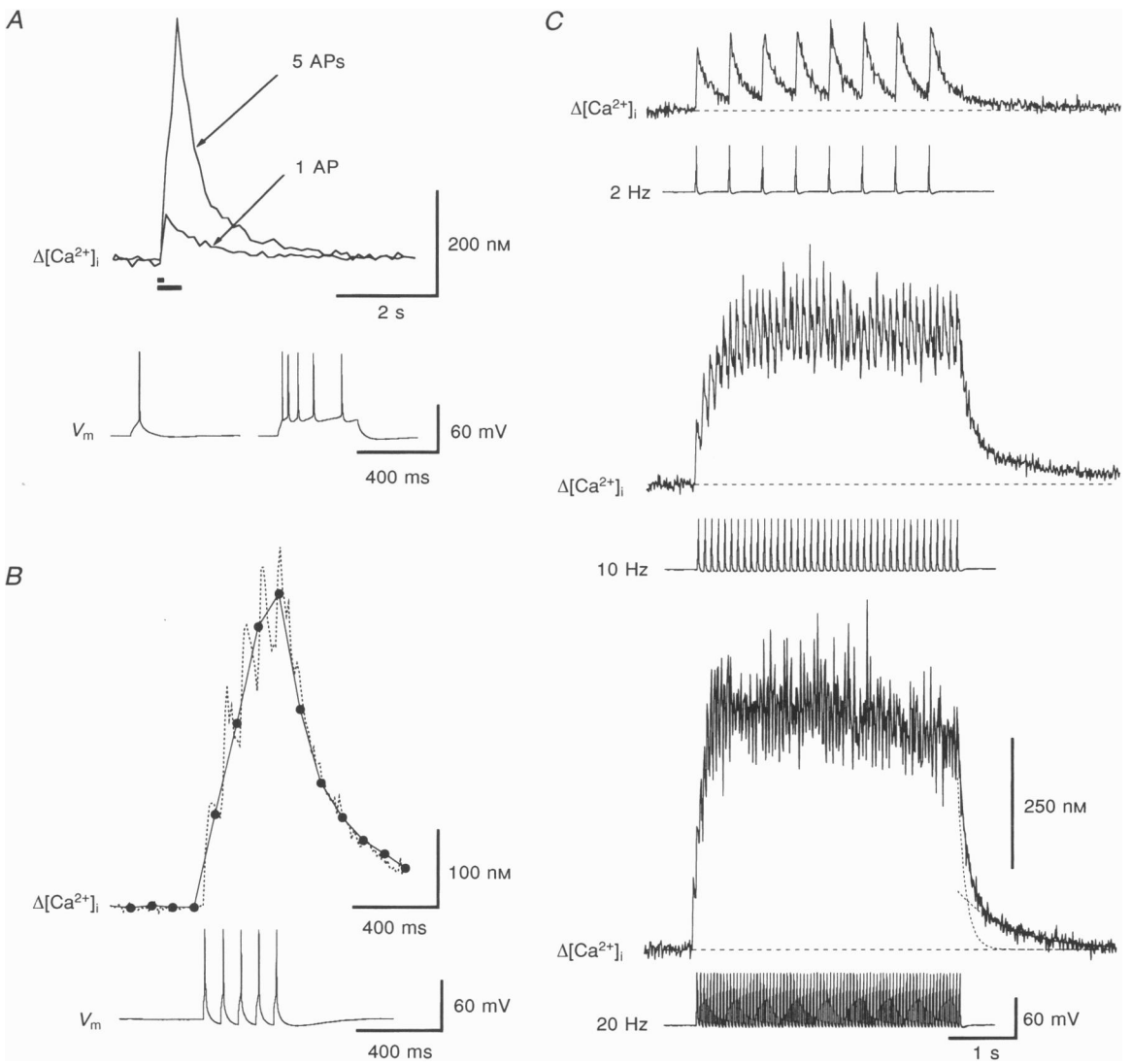

Figure 3. Dependence of $[Ca^{2+}]_i$ on AP frequency in the proximal dendrite

A, $[Ca^{2+}]_i$ transients evoked by a single AP (50 ms current injection) or a short burst of 5 APs (400 ms continuous current injection pulse) measured at 24 °C in the proximal apical dendrite (100 μm from the soma). Fluorescence acquisition rate was 10 Hz. *B*, comparison of the $[Ca^{2+}]_i$ transients measured with two different acquisition rates in the same ROI (apical dendrite, 100 μm from the soma). The continuous trace was measured at 10 Hz, the dotted trace at 100 Hz acquisition rate. The $[Ca^{2+}]_i$ transients were evoked by a short train of 5 APs at 24 °C (15 ms current injection pulses at 12 Hz, lower trace). *C*, accumulation of dendritic $[Ca^{2+}]_i$ during long trains of APs. Brief (5 ms) suprathreshold current pulses were delivered via the patch pipette at 2, 10 and 20 Hz for 4 s. $[Ca^{2+}]_i$ was measured in the proximal apical dendrite at 34 °C. A double exponential fit (continuous line) and its components (dashed lines, fast component 334 nM and 117 ms, slow component 114 nM and 767 ms) are shown for the decay of the $[Ca^{2+}]_i$ trace evoked by 20 Hz stimulation. Fluorescence signals were acquired at 100 Hz.

and fluorescence signals were acquired at 100 Hz. During the 2 Hz train of APs, little summation of the $[Ca^{2+}]_i$ transients was observed. At higher AP rates, $[Ca^{2+}]_i$ transients summed up and reached a plateau within about 250–500 ms at 10–20 Hz. The plateau level increased at higher rates and the mean level above resting reached during the last second of the stimulus was 77 ± 22 nM at 2 Hz, 287 ± 66 nM at 10 Hz, and 417 ± 108 nM at 20 Hz ($n = 7$). After the end of the high-frequency trains the decay of $[Ca^{2+}]_i$ could be well fitted with two exponential components. At 10 Hz, for example, the decay time constants were 157 ± 35 and 1440 ± 100 ms and the relative amplitudes of the two components were 80 and 20% ($n = 7$). At room temperature, $[Ca^{2+}]_i$ transients already began to summate at 2 Hz due to the longer decay of the single AP-evoked $[Ca^{2+}]_i$ transients at this

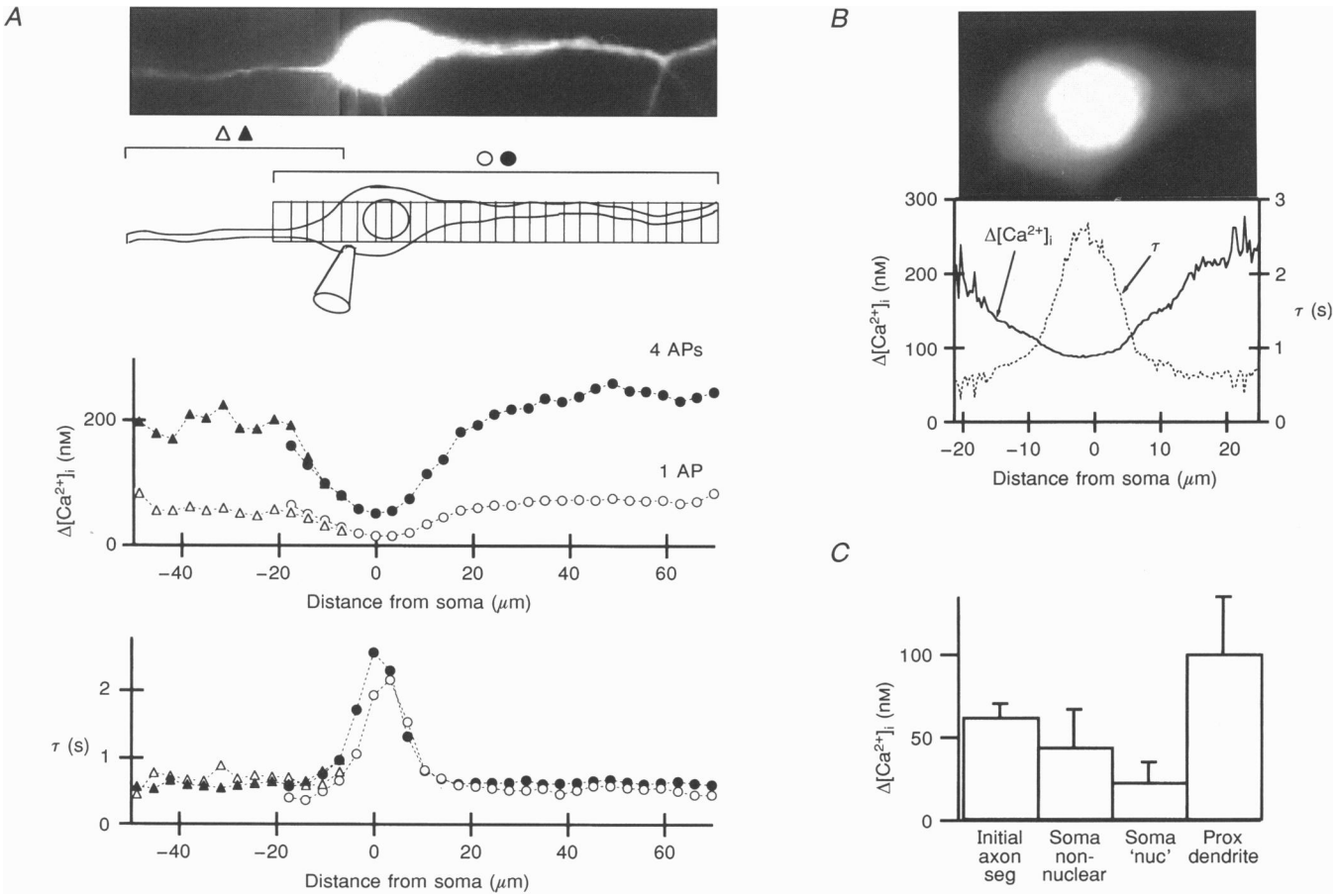

Figure 4. Spatial profile of AP-evoked $[Ca^{2+}]_i$ transients in soma, initial axon segment and proximal apical dendrite

A, fluorescence image of a neurone loaded with fura-2 via a somatic patch pipette is shown in the upper panel. $[Ca^{2+}]_i$ transients were evoked by 1 AP or 4 APs (50 and 400 ms current injection, respectively). Fluorescence signals were acquired at 20 Hz using the street-scan mode. Two regions (up to 90 μm in length) were selected, one including soma and proximal apical dendrite, the other including soma and initial axon segment (second panel). The regions were binned 'on-chip' in the vertical direction only. Ten pixels were averaged off-line to obtain a mean $[Ca^{2+}]_i$ transient every 3·5 μm (second panel). The decay of the transients was fitted by a single exponential. The third and fourth panels show the profile of peak and decay time constant of the $[Ca^{2+}]_i$ transients for both regions. Triangles represent the region which includes the soma and initial axon segment, circles the region including the soma and apical dendrite. Open symbols refer to 1 AP, closed symbols to 4 AP stimulation. Note that overlapping regions in the two street-scans give an almost identical profile. *B*, 'close-up' of the somatic region. Upper panel shows the somatic part of the fluorescence image enlarged. Fluorescence values were scaled to show differences in intensity within the somatic region. The lower panel shows the profile of peak and decay time constant of the $[Ca^{2+}]_i$ transients evoked by 4 APs. The $[Ca^{2+}]_i$ transients are presented in highest spatial resolution without off-line averaging (pixel size 0·35 μm). *C*, summary plot from 6 street-scan experiments presenting the means of $[Ca^{2+}]_i$ transient peaks measured in initial axon segment, non-nuclear somatic region, somatic region corresponding to the nucleus and proximal apical dendrite (up to 120 μm from the soma).

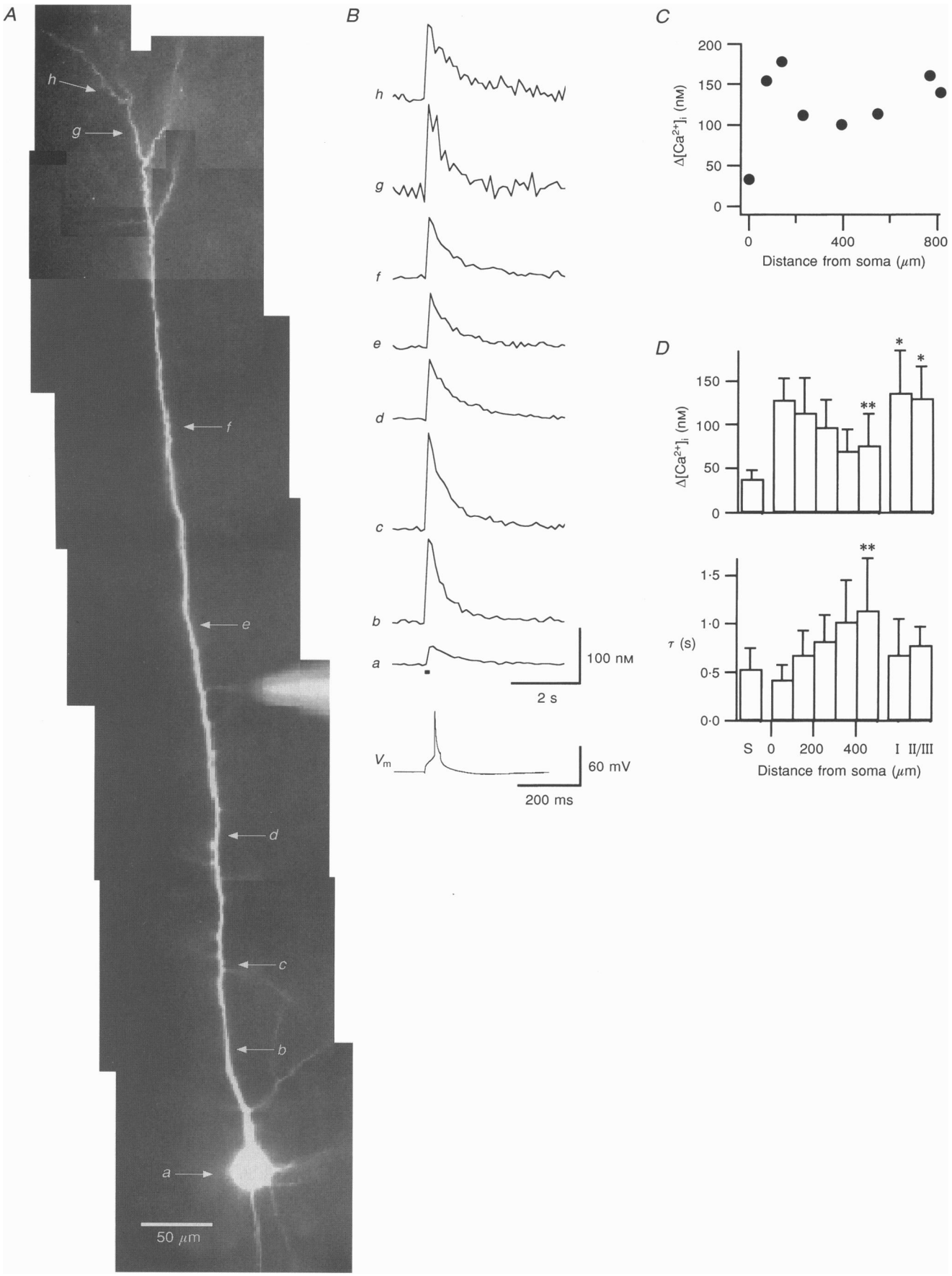

Figure 5. For legend see facing page.

temperature (see Fig. 2C). The mean $[Ca^{2+}]_i$ plateau levels were 720 ± 276 nM for 10 Hz and 938 ± 107 nM for 20 Hz ($n = 2$).

Differences in $[Ca^{2+}]_i$ transients between soma, initial axon segment and proximal apical dendrite

To examine further the spatial $[Ca^{2+}]_i$ profile of the proximal part of the neurone, we simultaneously measured $[Ca^{2+}]_i$ transients in the axon initial segment, the soma and the proximal apical dendrite using the 'street-scan' mode. A rectangular ROI was selected and binned in only one direction. Thus, high spatial resolution of $[Ca^{2+}]_i$ transients in the longitudinal direction of the ROI was obtained (see Methods).

Figure 4A presents $[Ca^{2+}]_i$ transient peaks and decay time constants as a function of the distance from the centre of the soma. The $[Ca^{2+}]_i$ transients measured in the proximal apical dendrite and initial segment of the axon were larger and decayed faster than those in the soma. These values were observed close to the 'origin' of both structures. Within both the measured axonal (up to 50 μm from the soma) and the measured dendritic portion (up to 70 μm from the soma), no significant inhomogeneities of the $[Ca^{2+}]_i$ transients were found. A similar spatial profile was obtained for $[Ca^{2+}]_i$ transients evoked by a train of four APs. Similar results were obtained in six neurones in which the proximal part of the neurone was measured simultaneously and no differences were observed between neurones filled via somatic ($n = 3$) or dendritic pipettes ($n = 3$).

Detailed analysis of the somatic region revealed differences in the $[Ca^{2+}]_i$ transient peak and decay time constant within the soma (Fig. 4B). The nucleus could be clearly visualized with IR-DIC video microscopy and appeared in the fluorescence image as a brighter structure. $[Ca^{2+}]_i$ transient peaks decreased gradually within the soma, having the lowest values in the area corresponding to the nucleus. The broadening of $[Ca^{2+}]_i$ transients was comparatively steep in the transition zone between the 'nuclear' and non-nuclear region. No significant difference in resting $[Ca^{2+}]_i$ concentrations was found between the 'nuclear' and non-nuclear region. Although $[Ca^{2+}]_i$ transient measurements from the 'nuclear' region represent signals from the nucleus and the cytoplasm above and below it, the difference in the fluorescence values between the two regions (2·5-fold) implies that the measured signal partially originated from the nucleus.

Figure 4C summarizes the mean values of the $[Ca^{2+}]_i$ transient peak obtained in the street-scan mode in the initial axon segment, 'nuclear' and non-nuclear somatic regions and the proximal apical dendrite, illustrating the clear differences between these subcellular compartments.

$[Ca^{2+}]_i$ transients in the dendritic tree

Synaptic terminals are located in all portions of the dendritic tree (White, 1989; Larkman, 1991; DeFelipe & Farinas, 1992). We therefore characterized the AP-evoked $[Ca^{2+}]_i$ transients in the different parts of the dendritic tree, including the fine dendritic branches such as the tuft branches, and the oblique and basal dendrites.

Fluorescence measurements in the fine dendritic branches of the dendritic tree present several technical difficulties arising mainly from the small volume of these branches and from the 3-dimensional structure of the dendritic tree, with changing focal planes. As a result, reliable $[Ca^{2+}]_i$ measurements in the small dendritic branches could not be

Figure 5. Spatial profile of $[Ca^{2+}]_i$ transients along the apical dendrite and dendritic tuft branches evoked by a single AP

A, a thick tufted layer V pyramidal neurone was loaded with fura-2 via a dendritic pipette located 340 μm from the soma. A collage of fluorescence images was made to show the entire neurone measured. Small ROIs (2–4 μm in width and 10 μm in length) were selected along the apical dendrite indicated by arrows. *B*, $[Ca^{2+}]_i$ transients measured in the various ROIs indicated in *A*, each evoked by a single AP (50 ms current injection, bottom trace shows the AP on an expanded time scale). $[Ca^{2+}]_i$ transients shown are means of 2–3 individual records. The lower signal-to-noise ratio in the fine branches (traces *g* and *h*) is mainly due to the small amount of dye contained in these thin structures. Fluorescence acquisition rate was 10 Hz. *C*, the peaks of the $[Ca^{2+}]_i$ transients shown in *B* are plotted as a function of distance from the soma. The second (ROI *g*) and third (ROI *h*) bifurcations are located around 760 and 800 μm from the soma, respectively. *D*, summary plot from 11 cells representing the mean profile of $[Ca^{2+}]_i$ transient peaks (upper graph) and decay time constants (lower graph) evoked by single APs in the soma and along the apical dendrite up to the third bifurcation. Along the main apical dendrite, data are pooled for every 100 μm of dendritic length into one bin. The sixth bin represents measurements from ROIs between 400 μm from the soma and the main bifurcation. Both peak amplitude and decay time constant in the sixth bin are significantly different from the values in the first dendritic bin (** represents $P < 0·001$). Compared with the sixth bin, the tuft branches show a significant difference in peak amplitudes (* represents $P < 0·01$) but not in decay time constants. S, soma; I, primary tuft branches; II/III, secondary and tertiary tuft branches.

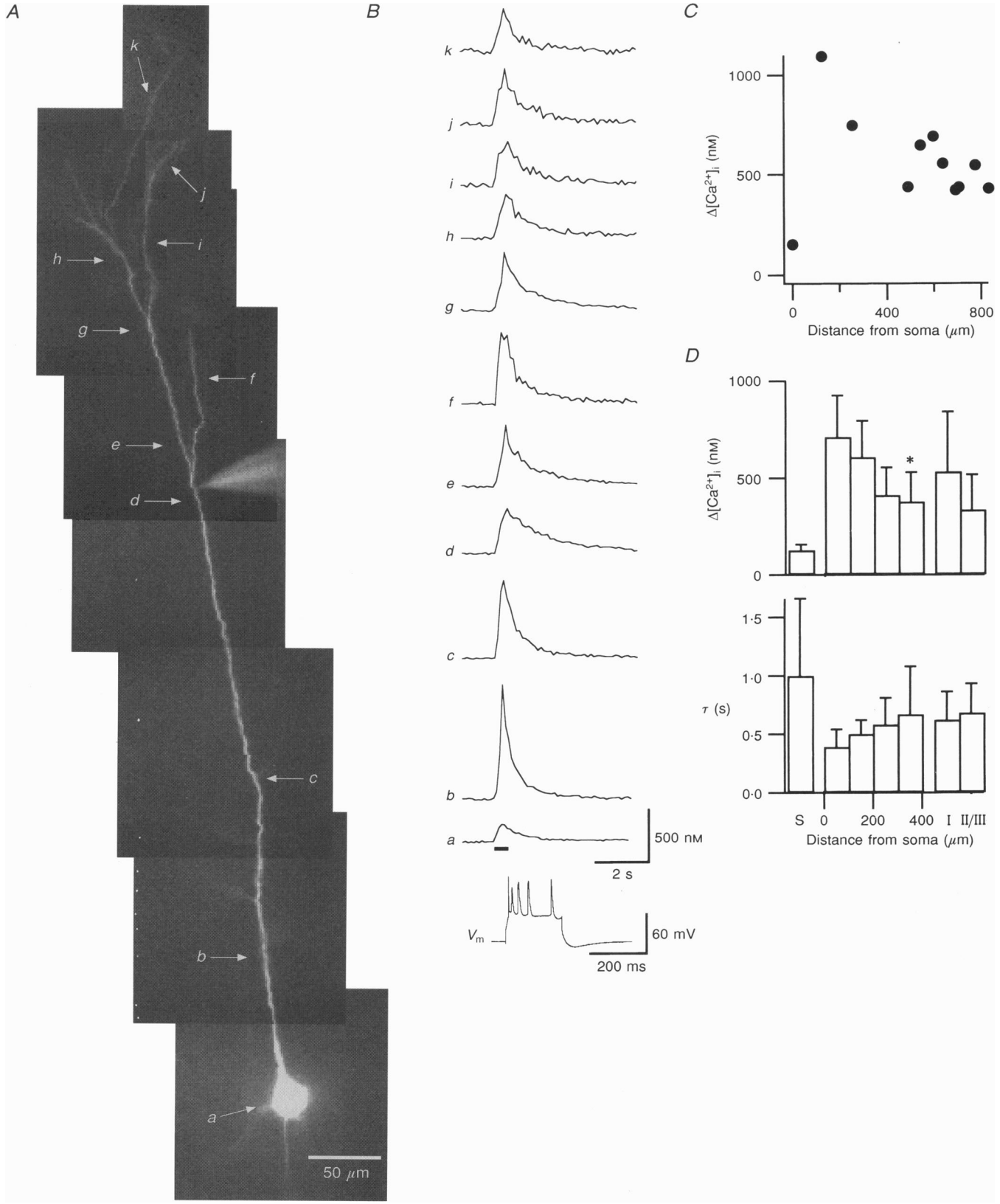

Figure 6. For legend see facing page.

obtained in the street-scan mode. However, measurements in the spot mode provided sufficient signal-to-noise ratio due to the on-chip binning (Lasser-Ross *et al.* 1991). Using this mode, however, the different regions of the dendritic tree were not measured simultaneously. To exclude time dependent processes, different portions of the dendrites were measured randomly and measurements in a few ROIs were repeated. Neurones in which the $[Ca^{2+}]_i$ transients changed with time (more than 10% change in the peak or decay time constant) were discarded (about 20% of the cells). In addition, we used a well-controlled stimulation regime and ensured the stability of the resting membrane potential.

$[Ca^{2+}]_i$ transients along the main apical dendrite and tuft branches

Figure 5 illustrates the spatio-temporal profile of $[Ca^{2+}]_i$ transients evoked by a single AP along the apical dendrite. The neurone was loaded with fura-2 via a patch pipette located 340 μm from the soma (Fig. 5*A*), providing rapid and reliable filling of distal dendrites.

Single APs evoked $[Ca^{2+}]_i$ transients along the entire main apical dendrite and the fine branches of the tuft (Fig. 5*B* and *C*). Figure 5*D* summarizes the mean values of $[Ca^{2+}]_i$ transient peak and decay time constant along the apical dendrite and the tuft branches from eleven neurones. In all experiments, $[Ca^{2+}]_i$ transients could be measured distal to the main bifurcation of the apical dendrite. On average, $[Ca^{2+}]_i$ transients reached a larger peak and decayed faster in the proximal part of the apical dendrite and gradually decreased in size and increased in duration up to the main bifurcation. The mean $[Ca^{2+}]_i$ transient peak measured in the proximal dendrite up to 100 μm from the soma was 128 ± 25 nM and the decay time constant was 420 ± 150 ms. In the distal part of the main apical dendrite, just proximal to the main bifurcation (more than 400 μm away from the soma), the $[Ca^{2+}]_i$ transient peak decreased to 76 ± 36 nM (59% of the value in the proximal dendrite, $P < 0{\cdot}001$) and the decay time constant was 1140 ± 540 ms (270% of the value in the proximal dendrite, $P < 0{\cdot}001$). In the finer branches of the dendritic tuft the $[Ca^{2+}]_i$ transients were larger than those measured proximal to the main bifurcation. In the primary branches, the $[Ca^{2+}]_i$ transient peak and decay time constant were 136 ± 48 nM and 680 ± 370 ms. In the secondary and tertiary tuft branches the values were not significantly different from those observed in the primary branches (130 ± 37 nM and 780 ± 190 ms). The differences in peak amplitudes between the tuft branches and the main apical dendrite proximal to the bifurcation were statistically significant ($P < 0{\cdot}01$).

To characterize the spatial profile of $[Ca^{2+}]_i$ transients evoked by a brief train of APs, 400–500 ms positive current pulses or trains of brief (30 ms) pulses were injected through the pipette. Figure 6*A–C* shows $[Ca^{2+}]_i$ transients evoked by a train of five APs along the main apical dendrite and in the primary, secondary and tertiary tuft branches of a pyramidal neurone. Figure 6*D* summarizes the results obtained from ten cells. Similar to the results obtained with single AP stimulation, $[Ca^{2+}]_i$ transients evoked by a train of five APs were larger in the proximal portion of the apical dendrite and gradually decreased in size along the dendrite. The $[Ca^{2+}]_i$ transient peaks measured proximal to the bifurcation were significantly smaller than those measured in the proximal dendrite ($P < 0{\cdot}05$). Decay time constants tended to be larger, but the difference was not statistically significant. Unlike single AP stimulation, $[Ca^{2+}]_i$ transients in the tuft branches were not significantly larger than those proximal to the main bifurcation.

The profile of the $[Ca^{2+}]_i$ transient may be influenced by a dye concentration gradient and differential wash-out of endogenous Ca^{2+} buffers. Two experimental findings

Figure 6. Spatial profile of $[Ca^{2+}]_i$ transients evoked by a short train of APs along the apical dendrite and dendritic tuft branches

A thick tufted layer V pyramidal cell was loaded via a dendritic pipette 490 μm from the soma. Experimental conditions were similar to those described in the previous figure except that the stimulation protocol consisted of a short train of 5 APs (500 ms current pulse). *A*, collage of fluorescence images showing the entire neurone measured. The locations of ROIs are indicated by arrows. *B*, $[Ca^{2+}]_i$ transients measured in the various ROIs indicated in *A*, each evoked by a train of 5 APs (bottom trace shows the train of APs on an expanded time scale). *C*, the peaks of the $[Ca^{2+}]_i$ transients shown in *B* are plotted as a function of distance from the soma. The third bifurcation point is located around 700 μm from the soma. *D*, summary plot from 10 cells presenting the mean profile of $[Ca^{2+}]_i$ transient peaks (upper graph) and decay time constants (lower graph) evoked by a train of 5 APs in the soma and along the apical dendrite up to the third bifurcation. Along the main apical dendrite data are pooled for every 100 μm of dendritic length into one bin. Peak amplitudes in the fifth bin (300–400 μm from soma) are significantly smaller than those in the first dendritic bin (* $P < 0{\cdot}05$). Peak amplitudes and decay time constants in the tuft branches show no significant difference compared with the values in the distal portion of the dendrite. S, soma; I, primary tuft branches; II/III, secondary and tertiary tuft branches.

indicate that this is not the case in our experiments. First, the profile was not dependent on the site of the filling pipette. Similar profiles were obtained with somatic pipettes (Fig. 7*A*) and dendritic pipettes located at different distances from the soma along the apical dendrite (100–490 μm). A double pipette filling experiment also showed the reduction of the $[Ca^{2+}]_i$ transient along the main apical dendrite (Fig. 7*B*). Second, the $[Ca^{2+}]_i$ transients in all experiments included did not change with time after an appropriate filling period (see Methods), indicating that both dye concentration and wash-out of buffers reached a steady state. However, we cannot exclude the possibility of a lower dye concentration in the very fine branches.

$[Ca^{2+}]_i$ transients in apical oblique and basal dendrites

Layer V pyramidal neurones typically possess oblique dendrites which branch off from the main apical trunk and basal dendrites which originate from the soma. Morphological studies estimate that about two-thirds of nerve terminals innervating a layer V pyramidal neurone terminate on the oblique and basal dendrites (Larkman, 1991; DeFelipe & Farinas, 1992). Therefore it was of interest to characterize the $[Ca^{2+}]_i$ transients in these fine dendritic branches.

To control for scattered light originating from the soma in the experiments on basal dendrites or from the main apical dendrite in the case of oblique dendrites, measurements were made only when oblique and basal dendrites were in the same focal plane as the soma and main apical dendrite, respectively. The selected ROIs were at least 10 μm distal to the origin of the basal and oblique dendrites. In addition, only experiments where the background fluorescence did not change during stimulation were included.

Figure 8*A* and *B* shows an example of $[Ca^{2+}]_i$ transients evoked by a single AP in an oblique dendrite and in the main apical dendrite adjacent to the branching point. The $[Ca^{2+}]_i$ transient was significantly larger and faster in the oblique dendrite compared with the main apical dendrite. Figure 8*C* summarizes the results obtained from nine neurones. On average, the $[Ca^{2+}]_i$ transient peak amplitude in oblique dendrites evoked by a single AP was 226 ± 69 nM and the decay time constant was 440 ± 170 ms ($n = 11$) compared with 92 ± 22 nM and 600 ± 240 ms ($n = 9$) in the corresponding main apical dendrites close to the origin of the oblique dendrites ($P < 0{\cdot}0001$ for $[Ca^{2+}]_i$ transient peaks and $P < 0{\cdot}01$ for decay time constants). A similar difference was observed when a short train of five APs was evoked. In five out of eleven oblique dendrites examined, $[Ca^{2+}]_i$ exceeded 1·5 μM, whereas $[Ca^{2+}]_i$ did not reach this value in any of the eight corresponding apical dendrites (mean peak was 494 ± 204 nM).

In basal dendrites the $[Ca^{2+}]_i$ transient evoked by a single AP or a short train of APs was also significantly larger and faster compared with that in the main apical dendrite (Fig. 8*D* and *E*). Figure 8*F* summarizes the results from twelve cells. On average, the $[Ca^{2+}]_i$ transient peak in the basal dendrite following a single AP was 267 ± 109 nM ($n = 15$) and the decay time constant was 470 ± 170 ms

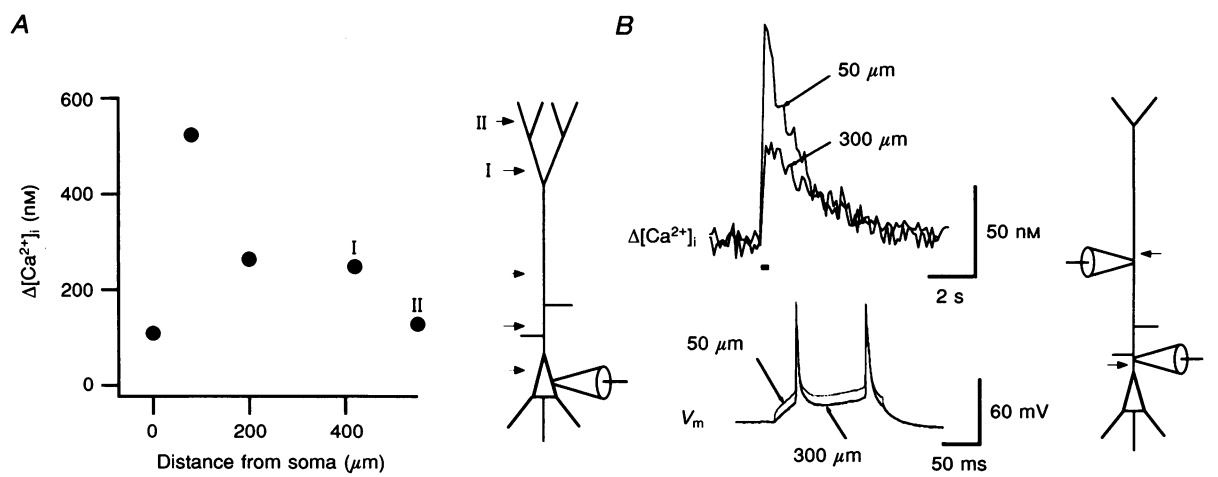

Figure 7. Differences in $[Ca^{2+}]_i$ transients along the apical dendrite do not depend on the site of the filling pipette

A, a layer V pyramidal cell was loaded via a somatic pipette. $[Ca^{2+}]_i$ transients were evoked by a train of 5 APs (30 ms current injection pulses at 12 Hz) and measured along the neurone (illustrated on the right). The $[Ca^{2+}]_i$ transient peaks are presented as a function of distance from the soma. I, primary tuft branches; II, secondary tuft branches. *B*, a layer V pyramidal cell was loaded using 2 pipettes, one located 50 μm from the soma, the other 300 μm from the soma (see illustration). $[Ca^{2+}]_i$ transients were evoked by 2 APs (150 ms current injection, bottom traces) and measured near the 2 pipettes (upper traces). Fluorescence acquisition rate was 10 Hz.

compared with 92 ± 30 nM ($n = 12$) and 670 ± 280 ms in the proximal apical dendrite up to 100 μm away from the soma ($P < 0.0001$ for peaks, and $P < 0.01$ for decay time constants). Following a train of five APs, in all thirteen basal dendrites examined $[Ca^{2+}]_i$ exceeded 1·5 μM whereas this value was not reached in any of the nine corresponding proximal apical dendrites (mean peak was 522 ± 253 nM).

Active dendritic AP propagation and $[Ca^{2+}]_i$ transients

To elucidate the role of active AP propagation in eliciting dendritic $[Ca^{2+}]_i$ transients in the apical and basal dendrites we compared $[Ca^{2+}]_i$ transients evoked by a short train of four to five APs measured under normal conditions with those evoked by a train of 'simulated' APs spreading passively into the dendritic tree. The train of APs recorded in the current-clamp mode was stored and used as a voltage command for voltage clamping the somatic membrane in the presence of TTX to block voltage-dependent Na^+ channels (Stuart & Sakmann, 1994).

Figure 9*A* and *B* compares the $[Ca^{2+}]_i$ transients measured in the soma and at two different locations along the main apical dendrite (100 and 300 μm from the soma) evoked by a train of actively propagating (control) or passively spreading APs (TTX). When Na^+ channels are blocked the mean $[Ca^{2+}]_i$ transient peak measured in the main apical dendrite 100 μm from the soma was reduced to 16% of control ($n = 5$), while 300 μm from the soma negligible or no $[Ca^{2+}]_i$ transients were observed ($n = 4$). In the experiments included, the somatic $[Ca^{2+}]_i$ transient was not reduced to more than 80% of the control value in the presence of TTX, indicating adequate voltage control at the soma during the simulated APs. Figure 9*C–F* shows similar experiments in basal dendrites. The degree of attenuation of the $[Ca^{2+}]_i$ transient in basal dendrites

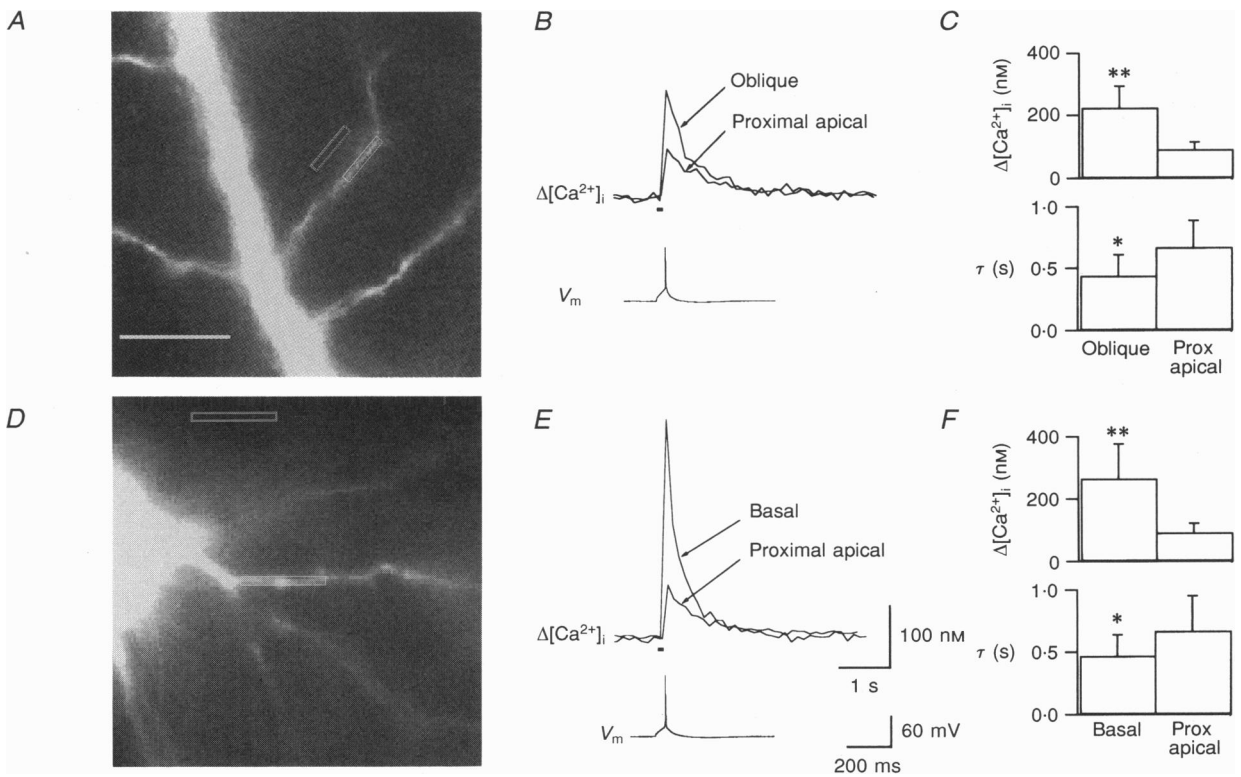

Figure 8. $[Ca^{2+}]_i$ transients in oblique and basal dendrites evoked by single APs

A, fluorescence image of oblique dendrites branching from the main apical dendrite in a layer V pyramidal neurone loaded with fura-2 (oblique ROI, single border; background ROI, double border). Scale bar (which also applies to *D*), 20 μm. *B*, $[Ca^{2+}]_i$ transients evoked by a single AP in an oblique dendrite and in the apical dendrite close to the origin of the oblique. *C*, mean of $[Ca^{2+}]_i$ transient peaks (upper graph) and decay time constants (lower graph) in oblique and parent apical dendrites evoked by single APs (9 cells were averaged). *D*, fluorescence image of basal dendrites and soma (basal ROI, single border; background ROI, double border). The ROI of the main apical dendrite was 50 μm distal from the soma (not shown). *E*, $[Ca^{2+}]_i$ transients evoked by a single AP in the basal dendrite and the main apical dendrite. *F*, mean of $[Ca^{2+}]_i$ transient peaks (upper graph) and decay time constants (lower graph) in basal dendrites and main apical dendrites evoked by single APs (12 cells were averaged). The single APs are shown in an expanded time scale, and the timing is indicated by the small filled bar. All measurements were done at 24 °C and 10 Hz fluorescence acquisition rate. Asterisks indicate statistical significance: * $P < 0.01$, ** $P < 0.0001$.

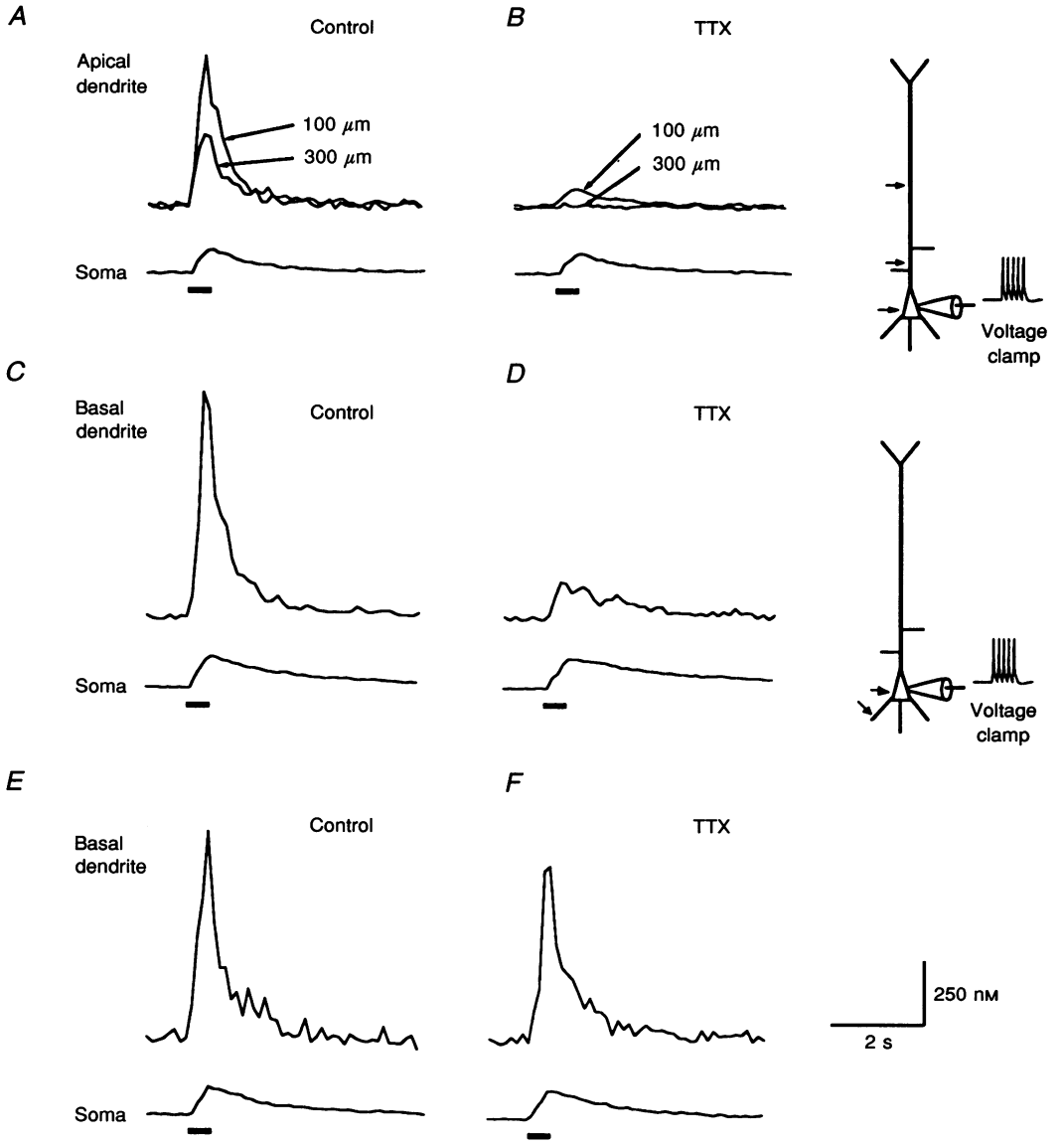

Figure 9. Active dendritic AP propagation and induction of $[Ca^{2+}]_i$ transients in apical and basal dendrites

Layer V pyramidal neurones were filled with fura-2 via somatic patch pipettes. $[Ca^{2+}]_i$ transients were evoked by a short train of 5 APs (12 Hz, evoked by brief current injections via the patch pipette). Later the slice was perfused with 1 μM TTX and the same train of APs recorded in control conditions was fed back into the soma in voltage-clamp mode. $[Ca^{2+}]_i$ transients were measured in the same ROIs as in control conditions. The $[Ca^{2+}]_i$ transients measured in the soma before and after the addition of TTX were used to control the reliability of the somatic waveform injection. In these experiments Sylgard-coated pipettes were used. The access resistance ranged between 5 and 8 MΩ (pipette resistance of 1·8–2·3 MΩ) and the series resistance compensation was set to 60–80%. *A* and *B*, effect of TTX on $[Ca^{2+}]_i$ transients measured in apical dendrite. $[Ca^{2+}]_i$ transients were measured in the soma and the main apical dendrite (100 and 300 μm from the soma) under normal conditions (Control, *A*) and in the presence of extracellular TTX (*B*). Note that somatic $[Ca^{2+}]_i$ transients in both conditions were not significantly different. The $[Ca^{2+}]_i$ transient in the presence of TTX was 12 and 8% of the control values 100 and 300 μm from the soma, respectively. *C–F*, effect of TTX on $[Ca^{2+}]_i$ transients measured in basal dendrites. $[Ca^{2+}]_i$ transients were measured in the soma and basal dendrites (75 and 80 μm from the soma) under normal conditions (Control, *C* and *E*) and in the presence of extracellular TTX (*D* and *F*). The two basal dendrites presented are from different cells. The change in the $[Ca^{2+}]_i$ transient measured in the basal dendrite in the presence of TTX differed between cells. The $[Ca^{2+}]_i$ transient in the basal dendrite shown in *C* and *D* was significantly reduced in the presence of TTX (16% of control) while that shown in *E* and *F* showed a much smaller change (84% of control). In both experiments the somatic $[Ca^{2+}]_i$ transient did not change significantly after the addition of TTX (94 and 100% of control).

showed larger variability, ranging from 16% (Fig. 9*C* and *D*) to 84% (Fig. 9*E* and *F*) of the control values. On average the $[Ca^{2+}]_i$ transient peak evoked by passively spreading APs in basal dendrites (50–80 μm from the soma) was 43% of control ($n = 4$).

DISCUSSION

The aim of the experiments reported was to determine the spatio-temporal profile of AP-evoked $[Ca^{2+}]_i$ transients in layer V pyramidal neurones of rat neocortex. The results indicate that pyramidal neurones are composed of several compartments with respect to the $[Ca^{2+}]_i$ transients evoked by suprathreshold stimulation. In the following sections, mechanisms which may underlie the spatial differences and possible functional implications are discussed.

Size and time course of $[Ca^{2+}]_i$ transients

The $[Ca^{2+}]_i$ transient peak is determined mainly by Ca^{2+} influx, the properties of Ca^{2+} buffers and the volume accessible to Ca^{2+} in the cellular compartment (Sala & Hernández-Cruz, 1990; Neher & Augustine, 1992; Zhou & Neher, 1993). The peak presumably represents a 'quasi-equilibrium' between $[Ca^{2+}]_i$ and the fast buffering system which is reached after Ca^{2+} influx through VDCCs has ceased and Ca^{2+} clearance is just beginning. The decay time course of the $[Ca^{2+}]_i$ transient is determined by Ca^{2+} clearance and by buffers. Lowering the fura-2 concentration below 150 μM increased the peak amplitude and shortened the decay of the $[Ca^{2+}]_i$ transient, indicating that at this concentration the indicator dye still affects the size and time course of the $[Ca^{2+}]_i$ transient. Nevertheless, this concentration was used to provide sufficient indicator filling of the fine dendritic branches.

The mean $[Ca^{2+}]_i$ transient peak in the proximal part of the apical dendrite evoked by a single AP was 113 ± 33 nM at 24 °C. This value could be an underestimate due to the additional fura-2 buffering capacity or an overestimate due to wash-out of mobile endogenous buffers through the patch pipette. Furthermore, $[Ca^{2+}]_i$ values depend on the calibration procedure converting fluorescence intensities to $[Ca^{2+}]_i$. Since the K_d of fura-2 could not be determined in cells, the exact $[Ca^{2+}]_i$ values remain uncertain and may be scaled linearly by a factor equal to the ratio of the K_d in neurones and in the pipette solution. The K_d values determined in cells range between 152 and 238 nM (Neher & Augustine, 1992; Zhou & Neher, 1993). Using the lower value would reduce the $[Ca^{2+}]_i$ values given here by a factor of 0·59. At more physiological temperatures (34 °C) $[Ca^{2+}]_i$ transients decayed faster, with a time constant of 300 ± 65 ms compared with 562 ± 212 ms at 24 °C. The faster decay presumably reflects the faster kinetics of Ca^{2+} clearance and Ca^{2+} buffers at 34 °C.

During trains of APs, intracellular Ca^{2+} concentration rises and reaches a plateau level which depends on the frequency. The fact that following 10–20 Hz stimulation $[Ca^{2+}]_i$ decays with two exponential components may indicate the recruitment of Ca^{2+} buffers with slower equilibration.

Spatial profile of AP-evoked $[Ca^{2+}]_i$ transients in axon initial segment, soma and proximal apical dendrite

The large difference in peak amplitude of $[Ca^{2+}]_i$ transients between the axon initial segment and the proximal apical dendrite on the one hand and the soma on the other could be caused by several factors such as differences in the surface-to-volume ratio, density or properties of VDCCs or endogenous buffers. The slower decay of $[Ca^{2+}]_i$ transients in the soma is possibly related to differences in the access of Ca^{2+} to clearance mechanisms, to the properties of clearance mechanisms or to the Ca^{2+} buffers. The results suggest that APs evoke $[Ca^{2+}]_i$ transients in the nucleus, which could link electrical activity to gene expression (Morgan & Curran, 1991). Nuclear $[Ca^{2+}]_i$ signals have been reported in other cells (Hernández-Cruz, Sala & Adams, 1990; Al-Mohanna, Caddy & Bolsover, 1994). The even slower $[Ca^{2+}]_i$ transient in the nuclear region could reflect less access to Ca^{2+} clearance, or accumulation of fura-2 in the nucleus. The gradual change in the $[Ca^{2+}]_i$ transient peak within the soma raises the possibility that the smaller peak in the 'nuclear' region is related to differences within the cytoplasm of the soma and not to differences between the nucleus and the surrounding cytoplasm.

Dendritic $[Ca^{2+}]_i$ compartments

The transient increase in $[Ca^{2+}]_i$ evoked by APs sweeps through the entire dendritic tree including the tuft branches and oblique and basal dendrites, indicating that APs invade the fine branches of the dendritic tree. A quantitative comparison of the $[Ca^{2+}]_i$ transient peaks shows large (up to 3·5-fold) differences between dendritic regions.

Along the main apical dendrite up to the main bifurcation, the $[Ca^{2+}]_i$ transient becomes progressively smaller and lasts longer. This is contrary to what is expected from simple considerations of changes in the surface-to-volume ratio assuming a hollow, smooth cylindrical structure, as the main apical dendrite decreases in diameter along its length (Larkman & Mason, 1990). The dendritic volume accessible to Ca^{2+} is, however, smaller than that estimated from the diameter since dendrites contain mitochondria and endoplasmic reticulum. Additionally, the fraction of the Ca^{2+}-accessible volume may differ between the proximal and distal parts of the dendrites.

Dendritic APs become smaller and longer as they propagate into the distal part of the apical dendrite (Figs 5 and 6 and Stuart & Sakmann, 1994). If dendritic Ca^{2+} channels have a high threshold for activation, the reduction in AP amplitude could cause a reduction in the Ca^{2+} influx despite the fact that the AP has a longer duration. This could, at least partially, explain the reduction of the $[Ca^{2+}]_i$ transient peak along the main apical dendrite. The contribution of other factors, such as differences in endogenous buffers,

subtypes of VDCCs and their density, remains to be elucidated.

The spatial profile of the $[Ca^{2+}]_i$ transient in the tuft branches is dependent on AP frequency. The single AP-evoked $[Ca^{2+}]_i$ transients are significantly larger in the tuft branches compared with the dendritic portion proximal to the main bifurcation. $[Ca^{2+}]_i$ transients in the tuft branches evoked by a train of APs show no significant increase, indicating that trains of APs may propagate less efficiently into distal dendritic branches.

Oblique and basal dendrites form an additional, separate compartment in which the AP-evoked $[Ca^{2+}]_i$ transient has the largest measured size, most probably reflecting an increased surface-to-volume ratio in these dendrites compared with the main apical dendrite, assuming smooth, hollow cylindrical structures. The differences between the oblique and basal dendrites on the one hand and the tuft branches on the other indicate that other factors such as differences in the electrical profile, density, or properties of VDCCs and properties of endogenous buffers may also contribute.

Dendritic AP propagation and $[Ca^{2+}]_i$ transients

In both the apical and basal dendrites, $[Ca^{2+}]_i$ transients evoked by passively spreading 'simulated' APs were significantly smaller compared with $[Ca^{2+}]_i$ transients measured under normal conditions, indicating that dendritic Na^+ channels are required to evoke dendritic $[Ca^{2+}]_i$ transients. The fact that the amplitude of passively spreading APs in the dendrite is significant (Stuart & Sakmann, 1994), and together with the marked reduction of AP-evoked $[Ca^{2+}]_i$ transients in the presence of TTX suggests that most of the AP-evoked Ca^{2+} influx is caused by activation of high-threshold VDCCs consistent with pharmacological studies (Markram, Helm & Sakmann, 1995).

Relation to previous work

Dendritic $[Ca^{2+}]_i$ transients were previously measured in hippocampal pyramidal neurones of the CA1 and CA3 region (Regehr, Connor & Tank, 1989; Jaffe *et al.* 1992; Regehr & Tank, 1992), cerebellar Purkinje neurones (Ross & Werman, 1987; Tank, Sugimori, Connor & Llinás, 1988; Lev-Ram *et al.* 1992) and pyramidal neurones of cortical layer V (Markram & Sakmann, 1994; Yuste, Gutnick, Saar, Delaney & Tank, 1994). A quantitative comparison with the results reported here is difficult because of differences in stimulation, dye concentration and methods of calibration, but qualitative differences in spatial $[Ca^{2+}]_i$ profiles are apparent.

Yuste *et al.* (1994) described an increased Ca^{2+} accumulation in the middle portion of the apical dendrite of layer V neocortical pyramidal neurones during antidromic or synaptic stimulation, which was tentatively attributed to an increased Ca^{2+} influx in this region. The results reported here do not confirm higher $[Ca^{2+}]_i$ accumulation in this region. In fact, the $[Ca^{2+}]_i$ transient peak measured in the middle portion of the apical dendrite, proximal to the main bifurcation, was the lowest measured in the dendritic tree. The smaller $[Ca^{2+}]_i$ accumulation in the proximal apical dendrite reported by Yuste *et al.* (1994) may be due to

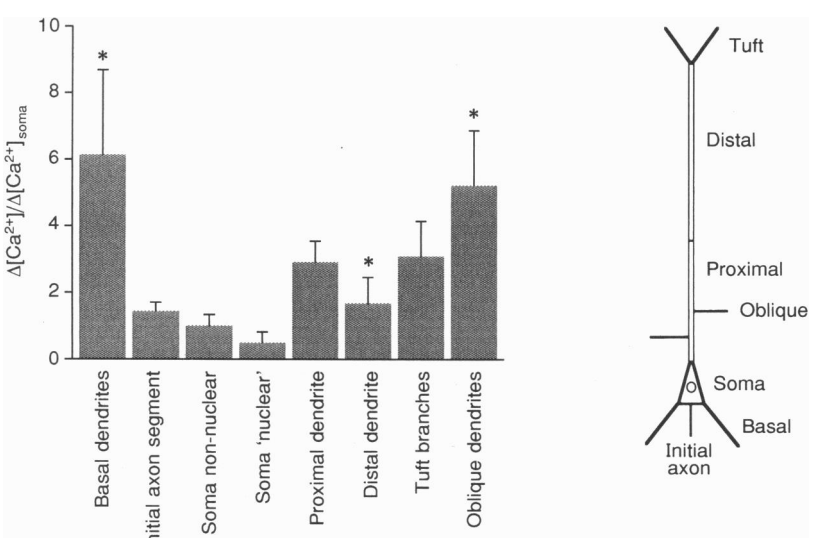

Figure 10. Summary plot of the peak $[Ca^{2+}]_i$ profile evoked by a single AP in a typical thick tufted layer V pyramidal neurone

The mean values of $[Ca^{2+}]_i$ transient peak amplitudes in the different regions of the neurone are presented. The values are normalized to the mean amplitude in the non-nuclear region of the soma. The scheme illustrates the different portions of the pyramidal neurone which were measured. Within the dendritic tree, the peak amplitudes in all compartments, except in the tuft branches, are significantly different from those in the proximal dendrite (* $P < 0{\cdot}001$).

overloading by high fura-2 concentration and a concentration gradient along the dendrite. This view is supported by the very slow decay time of the $[Ca^{2+}]_i$ transients. The apparent reduction in $[Ca^{2+}]_i$ accumulation at distal apical dendrites is possibly caused by frequency-dependent reduction in the propagation of APs into distal apical dendrites during high-frequency stimulation. Other factors such as lower optical resolution and slow temporal resolution of ratiometric measurements may also contribute to the differences in the profiles.

The spatial profile of AP-evoked $[Ca^{2+}]_i$ transients in hippocampal pyramidal neurones and cerebellar Purkinje neurones differs significantly from that in cortical pyramidal neurones. In hippocampal neurones the dendritic $[Ca^{2+}]_i$ transient was largest in the proximal apical dendrite (the initial dendritic portion up to 100 μm distal to the soma) and gradually decreased in size along the main apical dendrite until undetectable levels were reached at about 250 μm from the soma (Jaffe *et al.* 1992; Regehr & Tank, 1992; Jaffe, Ross, Lisman, Lasser-Ross, Miyakawa & Johnston, 1994). In cerebellar Purkinje neurones, dendritic $[Ca^{2+}]_i$ transients were not observed in the distal dendrites following somatic, Na^+-dependent APs. Large dendritic $[Ca^{2+}]_i$ transients were, however, evoked following the activation of dendritic Ca^{2+}-dependent APs (Tank *et al.* 1988; Lev-Ram *et al.* 1992). The difference between the three classes of neurones is possibly due to differences in the degree of back-propagation of Na^+-dependent APs into their dendritic tree (Jaffe *et al.* 1992; Stuart & Sakmann, 1994; Stuart & Häusser, 1994).

Functional significance of dendritic $[Ca^{2+}]_i$ compartments

The spatial profile of AP-evoked $[Ca^{2+}]_i$ transients is inhomogeneous, being of largest amplitude in oblique and basal dendrites and lowest in the soma (Fig. 10). Since $[Ca^{2+}]_i$ may influence synaptic efficacy and integration of inhibitory and excitatory synaptic potentials (Inoue *et al.* 1986; Mayer *et al.* 1987; Taleb *et al.* 1987; Malenka, Kauer, Zucker & Nicoll, 1988; Llano *et al.* 1991; Bliss & Collingridge, 1993; Wyllie, Manabe & Nicoll, 1994), the different size of $[Ca^{2+}]_i$ transients developing in the various portions of the neurone will have differential effects on synaptic transmission, depending on the location of synapses. This assumes that the AP-evoked Ca^{2+} influx causes $[Ca^{2+}]_i$ to rise in the vicinity of postsynaptic membrane areas, for example in dendritic spines. Of the excitatory synapses which innervate a thick tufted layer V pyramidal neurone, approximately 40% are formed with basal dendrites, 25% with oblique dendrites, 20% with the main apical dendrite and about 10% with the tuft branches (White, 1989; Larkman, 1991; DeFelipe & Farinas, 1992). Some of the afferents to neocortical pyramidal neurones selectively terminate on specific portions of the dendritic tree. For example, thalamocortical afferents terminate mainly on dendrites of layers IV and VI, and reciprocal associational cortico-cortical afferents preferentially innervated the tuft branches (White, 1989; Cauller & Connors, 1994). Selective innervation is also well established for inhibitory inputs, since chandelier cells innervate the axon initial segment and many of the axonal endings of neocortical basket cells terminate on the soma (White, 1989; DeFelipe & Farinas, 1992).

Finally, the frequency dependence of dendritic Ca^{2+} accumulations may signal to dendrites the level of the actual neuronal output activity. Since the $[Ca^{2+}]_i$ transients depend differentially on the frequency of back-propagating APs in different portions of the dendritic tree, the $[Ca^{2+}]_i$ compartments are dynamic and depend on neuronal activity. Therefore the relative efficacy of synaptic transmission in different portions of the dendritic tree may also depend on ongoing electrical activity. Further questions arising from the present results are whether back-propagating APs also increase $[Ca^{2+}]_i$ in dendritic spines, possibly via VDCCs in the spine head, and what is the relative amplitude of dendritic $[Ca^{2+}]_i$ transients mediated via VDCCs and Ca^{2+} permeable *N*-methyl-D-aspartate (NMDA) glutamate receptors.

Alloway, K. D., Johnson, M. J. & Wallace, M. B. (1993). Thalamocortical interactions in the somatosensory system: Interpretations of latency and cross-correlation analysis. *Journal of Neurophysiology* **70**, 892–908.

Al-Mohanna, F. A., Caddy, K. W. T. & Bolsover, S. R. (1994). The nucleus is insulated from cytosolic calcium ion changes. *Nature* **367**, 745–750.

Artola, A. & Singer, W. (1993). Long-term depression of excitatory synaptic transmission and its role in long term potentiation. *Trends in Neurosciences* **16**, 480–487.

Blatz, A. L. & Magleby, K. L. (1987). Calcium activated potassium ion channels. *Trends in Neurosciences* **11**, 438–443.

Bliss, T. V. P. & Collingridge, G. L. (1993). A synaptic model of memory: long-term potentiation in the hippocampus. *Nature* **361**, 31–39.

Cauller, L. J. & Connors, B. W. (1994). Synaptic physiology of horizontal afferents to layer I in slices of rat SI neocortex. *Journal of Neuroscience* **14**, 751–762.

DeFelipe, J. & Farinas, I. (1992). The pyramidal neuron of the cerebral cortex: morphological and chemical characteristics of the synaptic inputs. *Progress in Neurobiology* **39**, 563–607.

Grynkiewicz, G., Poenie, M. & Tsien, R. Y. (1985). A new generation of Ca^{2+} indicators with greatly improved fluorescence properties. *Journal of Biological Chemistry* **260**, 3440–3450.

Hernández-Cruz, A., Sala, F. & Adams, P. R. (1990). Subcellular calcium transients visualized by confocal microscopy in a voltage-clamped vertebrate neuron. *Science* **247**, 858–862.

Inoue, M., Oomura, Y., Yakushiji, T. & Akaike, N. (1986). Intracellular calcium ions decrease the affinity of the GABA receptor. *Nature* **324**, 156–158.

Jack, J. J. B., Noble, D. & Tsien, R. W. (1983). *Electrical Current Flow in Excitable Cells.* Oxford University Press, Oxford.

JAFFE, D. B., JOHNSTON, D., LASSER-ROSS, N., LISMAN, J. E., MIYAKAWA, H. & ROSS, W. N. (1992). The spread of Na^+ spikes determines the pattern of dendritic Ca^{2+} entry into hippocampal neurons. *Nature* **357**, 244–246.

JAFFE, D. B., ROSS, W. N., LISMAN, J. E., LASSER-ROSS, N., MIYAKAWA, H. & JOHNSTON, D. (1994). A model for dendritic Ca^{2+} accumulation in hippocampal neurons based on fluorescence imaging measurements. *Journal of Neurophysiology* **71**, 1065–1077.

LANCASTER, B. & NICOLL, R. A. (1987). Properties of two calcium-activated hyperpolarizations in rat hippocampal neurons. *Journal of Physiology* **389**, 187–203.

LANCASTER, B. & ZUCKER, R. S. (1994). Photolytic manipulation of Ca^{2+} and the time course of slow, Ca^{2+}-activated K^+ current in rat hippocampal neurons. *Journal of Physiology* **475**, 229–239.

LARKMAN, A. U. (1991). Dendritic morphology of pyramidal neurons of the rat: Spine distribution. *Journal of Comparative Neurology* **306**, 332–343.

LARKMAN, A. U. & MASON, A. (1990). Correlations between morphology and electrophysiology of pyramidal neurons in slices of rat visual cortex. I. Establishment of cell classes. *Journal of Neuroscience* **10**, 1407–1414.

LASSER-ROSS, N., MIYAKAWA, H., LEV-RAM, V., YOUNG, S. R. & ROSS, W. N. (1991). High time resolution fluorescence imaging with a CCD camera. *Journal of Neuroscience Methods* **36**, 253–261.

LATTANZIO, F. A. & BARTSCHAT, D. K. (1991). The effect of pH on rate constants, ion selectivity and thermodynamic properties of fluorescent calcium and magnesium indicators. *Biochemical and Biophysical Research Communication* **177**, 184–191.

LEV-RAM, V., MIYAKAWA, H., LASSER-ROSS, N. & ROSS, W. N. (1992). Calcium transients in cerebellar Purkinje neurons evoked by intracellular stimulation. *Journal of Neurophysiology* **68**, 1167–1177.

LLANO, I., LERESCHE, N. & MARTY, A. (1991). The entry of calcium increases the sensitivity of cerebellar Purkinje cells to applied GABA and decreases inhibitory synaptic currents. *Neuron* **6**, 565–574.

MALENKA, R. C., KAUER, J. A., ZUCKER, R. S. & NICOLL, R. A. (1988). Postsynaptic calcium is sufficient for potentiation of hippocampal synaptic transmission. *Science* **242**, 81–84.

MARKRAM, H., HELM, P. J. & SAKMANN, B. (1995). Dendritic calcium transients evoked by single back-propagating action potentials in neocortical pyramidal neurons. *Journal of Physiology* **485**, 1–20.

MARKRAM, H. & SAKMANN, B. (1994). Calcium transients in apical dendrites evoked by single subthreshold excitatory postsynaptic potentials via low-voltage-activated calcium channels. *Proceedings of the National Academy of Sciences of the USA* **91**, 5207–5211.

MAYER, M. L., MACDERMOTT, G. L., WESTBROOK, G. L., SMITH, S. J. & BARKER, J. L. (1987). Agonist- and voltage-gated calcium entry in cultured mouse spinal cord neurons under voltage clamp measured using arsenazo 3. *Journal of Neuroscience* **7**, 3230–3244.

MORGAN, J. L. & CURRAN, T. (1991). Stimulus-transcription coupling in the nervous system: involvement of the inducible proto-oncogenes *fos* and *jun*. *Annual Review of Neuroscience* **14**, 421–445.

NEHER, E. & AUGUSTINE, G. J. (1992). Calcium gradients and buffers in bovine chromaffin cells. *Journal of Physiology* **450**, 273–301.

RALL, W. (1967). Distinguishing theoretical synaptic potentials computed for different soma-dendritic distributions of synaptic input. *Journal of Neurophysiology* **30**, 1138–1168.

REGEHR, W. G., CONNOR, J. A. & TANK, D. W. (1989). Optical imaging of calcium accumulation in hippocampal pyramidal cells during synaptic activation. *Nature* **341**, 533–536.

REGEHR, W. G. & TANK, D. W. (1992). Calcium concentration dynamics produced by synaptic activation of CA1 hippocampal pyramidal cells. *Journal of Neuroscience* **12**, 4202–4223.

ROSS, W. N. & WERMAN, R. (1987). Mapping calcium transients in the dendrites of Purkinje cells from the guinea-pig cerebellum *in vitro*. *Journal of Physiology* **389**, 319–336.

SALA, F. & HERNÁNDEZ-CRUZ, A. (1990). Calcium diffusion modelling in a spherical neuron. Relevance of buffering properties. *Biophysical Journal* **57**, 313–324.

SPRUSTON, N., JAFFE, D. B. & JOHNSTON, D. (1994). Dendritic attenuation of synaptic potentials and currents: the role of passive membrane properties. *Trends in Neurosciences* **17**, 161–166.

STUART, G. J., DODT, H.-U. & SAKMANN, B. (1993). Patch-clamp recordings from the soma and dendrites of neurons in brain slices using infrared video microscopy. *Pflügers Archiv* **423**, 511–518.

STUART, G. J. & HÄUSSER, M. (1994). Initiation and spread of sodium action potentials in cerebellar Purkinje cells. *Neuron* **13**, 703–712.

STUART, G. J. & SAKMANN, B. (1994). Active propagation of somatic action potentials into neocortical pyramidal cell dendrites. *Nature* **367**, 69–72.

TALEB, O., TROULARD, J., DEMENEIX, B. A., FELTZ, P., BOSSU, J.-L., DUPONT, J.-L. & FELTZ, A. (1987). Spontaneous and GABA-evoked chloride channels on pituitary intermediate lobe cells and their internal Ca requirements. *Pflügers Archiv* **409**, 620–631.

TANK, D. W., SUGIMORI, M., CONNOR, J. A. & LLINÁS, R. R. (1988). Spatially resolved calcium dynamics of mammalian Purkinje cells in cerebellar slice. *Science* **242**, 773–777.

WHITE, E. L. (1989). *Cortical Circuits*. Birkhäuser, Boston, MA, USA.

WYLLIE, D. J. A., MANABE, T. & NICOLL, R. A. (1994). A rise in postsynaptic Ca^{2+} potentiates miniature excitatory postsynaptic currents and AMPA responses in hippocampal neurons. *Neuron* **12**, 127–138.

YUSTE, R., GUTNICK, M. J., SAAR, D., DELANEY, K. R. & TANK, D. W. (1994). Ca^{2+} accumulations in dendrites of neocortical pyramidal neurons: an apical band and evidence for two functional compartments. *Neuron* **13**, 23–43.

ZHOU, Z. & NEHER, E. (1993). Mobile and immobile calcium buffers in bovine adrenal chromaffin cells. *Journal of Physiology* **469**, 245–273.

Acknowledgements

We thank Drs K. Imoto, H. Markram, Y. Schiller, N. Spruston and G. Stuart for critically reading the manuscript, M. Kaiser for technical assistance and H. Spiegel for typing the manuscript. This work was supported by the Minerva Foundation (J.S.).

Received 6 December 1994; accepted 24 February 1995.